ELSEVIER

Chemical Engineering Science 60 (2005) 1085–1101

Chemical Engineering Science

www.elsevier.com/locate/ces

Numerical simulation of bubble columns flows: effect of different breakup and coalescence closures

P. Chen[a], J. Sanyal[b], M.P. Dudukovic[a,*]

[a]*Chemical Reaction Engineering Laboratory, Department of Chemical Engineering, Washington University, One Brookings Drive, Box 1198, St. Louis, MO 63130-4899, USA*
[b]*Fluent Inc., Lebanon, NH 03766-1442, USA*

Received 19 December 2003; received in revised form 31 August 2004; accepted 9 September 2004

Abstract

Two-dimensional axisymmetric Eulerian/Eulerian simulations of two-phase (gas/liquid) transient flow were performed using a multiphase flow algorithm based on the finite-volume method. These numerical simulations cover laboratory scale bubble columns of different diameters, operated over a range of superficial gas velocities ranging from the bubbly to the churn turbulent regime. The bubble population balance equation (BPBE) is implemented in the two-fluid model that accounts for the drag force and employs the modified k–ε turbulence model in the liquid phase. Several available bubble breakup and coalescence closures are tested. Quantitative agreements between the experimental data and simulations are obtained for the time-averaged axial liquid velocity profiles, as well as for the kinetic energy profiles, only when model predicted breakup rate is increased by a factor of ten to match the coalescence rate. The calculated time-averaged gas holdup profiles deviate in shape from the measured ones and suggest that full three-dimensional simulation is needed. Implementation of BPBE leads to better agreement with data, especially in the churn-turbulent flow regime, compared to the simulation based on an estimated constant mean bubble diameter. Differences in the predicted interfacial area density, with and without BPBE implementation, are significant. The choice of bubble breakup and coalescence closure does not have a significant impact on the simulated results as long as the magnitude of breakup is increased tenfold.
© 2004 Elsevier Ltd. All rights reserved.

Keywords: Bubble columns; Computational fluid dynamics; Dynamic simulation; Population balance; Modeling; Multiphase flow

1. Introduction

Bubble column reactors are widely used in a variety of industries such as for Fischer–Tropsch synthesis, in fine chemicals production, in oxidation and hydrogenation reactions, in coal liquefaction, in fermentation and, more recently, in cell cultures, waste water treatment and single cell protein production. The primary advantages of bubble column reactors are easy construction due to no moving parts (which leads to easier maintenance), high gas–liquid interfacial area, good mass/heat transfer rate between gas and liquid phase, and large liquid holdup which is favorable for slow liquid phase reactions (Shah et al., 1982). The operation of bubble column reactors is affected by global operating parameters such as gas superficial velocity, operating pressure and temperature, and liquid height. The many hydrodynamic variables that influence bubble column performance are: gas holdup distribution, bubble breakup, coalescence and dispersion rate, bubble rise velocity, bubble size distribution, gas–liquid interfacial area concentration distribution, gas–liquid mass/heat transfer coefficients and the extent of liquid phase backmixing (Krishna et al., 1996; Dudukovic et al., 1997). In design, scale-up and scale-down of such reactors the understanding of the fluid dynamics is a critical issue. One should stress that from the industrial point of view churn-turbulent flow is of most interest as it ensures high volumetric productivity.

* Corresponding author. Tel.: +1 314 935 6021; fax: +1 314 935 4832.
E-mail address: dudu@che.wustl.edu (M.P. Dudukovic).

0009-2509/$ - see front matter © 2004 Elsevier Ltd. All rights reserved.
doi:10.1016/j.ces.2004.09.070

The dynamics of gas–liquid flows has been a topic of research for the last several decades. Various methods are available for the simulation of dispersed two-phase flows. They range from model-free direct numerical simulations (DNS) (Druzhinin and Elghobashi, 1998; Bunner and Tryggvason, 1999; Joseph, 2002) to continuum-based models requiring a considerable number of closure relationships (Kashiwa and Rauenzahn, 1994; Lahey and Drew, 2001). In principle, multiphase flow can be mathematically described by the basic equations of fluid mechanics. However, due to excessive cost and unavailability of fast enough computers, DNS simulations are unsuitable for practical industrial situations. For similar reasons, the Eulerian–Lagrangian approach (e.g. Lapin and Lübbert, 1994; Delnoij et al., 1997) has been limited to the situation where the gas velocity and gas holdup is relatively low. The Eulerian–Eulerian approach (e.g., Drew, 1983; Torvik and Svendsen, 1990; Sokolichin and Eigenberger, 1994; Krishna et al., 2000; Pan et al., 2000), also referred to as the two-fluid model, describes the motion of the two-phase mixture in a macroscopic sense. To model the drag force term, which is one of the key closures, most numerical simulations resort to a single particle model with a so-called "mean" bubble size (e.g. Sokolichin and Eigenberger, 1994; Pan et al., 2000). This is mostly done because modeling different sizes of bubbles as individual phases leads to unrealistic computational cost and has numerical convergence problems. The assumption of a single bubble size is justified in bubbly flow because bubble–bubble interactions are weak and bubble sizes are narrowly distributed. However, in churn-turbulent flow, where most industrial applications lie, bubble–bubble interactions result in widely distributed bubble sizes that may be substantially different from the "mean" bubble size assumption. In addition, in order to generate a simulation result that resembles available data, the "mean" bubble size is customarily adjusted by a trial-and-error procedure and the value so chosen often is far from reality. To overcome this problem, Krishna and coauthors (e.g., Krishna et al., 2000; van Baten and Krishna, 2001) have introduced the concept of two bubble classes ("large" and "small" bubbles) for churn-turbulent flow and prescribed phenomenological relations for evaluation of the representative size of the two classes and their volume fractions.

There still is a need, when evaluating the performance of existing bubble column reactors and when designing new ones in churn-turbulent flow, to assess the gas holdup radial distribution, because it drives liquid recirculation, and local interfacial area concentration distribution, because it is essential to mass transfer. An engineering level of accuracy is needed. Based on extensive studies by many authors, we know that the two-fluid model based codes (e.g. FLUENT, CFX, CFDLIB, etc.) that utilize the mean bubble size concept cannot predict well the observed gas holdup radial profiles even in 3D simulation while the predicted velocity profiles and overall gas holdup estimates are pretty good (Pan and Dudukovic, 2001). Some improvement is acclaimed by Krishna et al. (2000) who used two bubble classes of constant size without inter-class interaction throughout the column.

Moreover, available estimates of the local interfacial area are based on the predicted local gas holdup and assumed mean bubble size and are likely in error. To remedy this situation, the implementation of the bubble population balance model (BPBE) in the Eulerian–Eulerian model is needed. This eliminates the assumption of either single constant bubble size or of small and large bubble and possibly may improve the gas holdup profile prediction. Most importantly, the implementation of BPBE allows one to predict the bubble size distribution locally, and eliminates the trial-and-error procedure regarding the assignment of unknown mean bubble diameter mentioned above, while providing the capability of predicting the interfacial area concentration locally throughout the column.

We try to implement the bubble population balance equation (BPBE) in the Euler–Euler CFD representation to assess how well we can predict liquid velocity and gas holdup profiles, as well as gas–liquid interfacial area and liquid back mixing. The first two are compared with the available experimental data.

2. Experimental data

At the Chemical Reaction Engineering Laboratory, Washington University in St. Louis, the unique CARPT-CT facilities allow non-invasive monitoring of the velocity and holdup profiles of two phases in opaque multiphase system on a single platform (Devanathan et al., 1990; Yang et al., 1992b; Kumar et al., 1997; Degaleesan, 1997; Chen et al., 1999; Degaleesan et al., 2001).

In a set of cylindrical air–water bubble columns, Degaleesan (1997) experimentally studied the time-averaged velocity and turbulence parameters of the liquid phase by using the Computer Automated Radioactive Particle Tracking (CARPT) Technique. CARPT is a non-invasive technique for tracking the trajectory of a radioactive particle. In CARPT, one resorts to tagging the "typical fluid element" with a gamma ray source (i.e., the liquid phase is tagged with a neutrally buoyant radioactive particle containing Scandium-46). The particle location at each time instant, $\mathbf{x}_p(t)$, can be reconstructed from a record of the gamma-ray photon counts at a number of strategically located NaI scintillating detectors, and a pre-established calibration between the detector counts and tracer particle location. Tracer particle trajectory is acquired over a very long time, typically 18–20 h, in order to collect sufficient statistics (typically, two million or more occurrences in the column). By time differencing of successive particle positions one obtains the instantaneous Lagrangian particle velocity, $\mathbf{u}_p(t)$, and cross-correlation of these can be used to compute the components of the turbulent eddy diffusivity tensor (Devanathan et al., 1990; Yang et al., 1992a; Degaleesan, 1997).

The time-averaged liquid velocities and turbulence parameters in the Eulerian framework, i.e., at different positions in the column, can be calculated from CARPT data. The column is divided into compartments. The velocity of the particle is then assigned to that compartment which contains the mid-point of the two successive positions of the particle. In this manner instantaneous velocities are assigned to their respective compartments. Ensemble averaging is done of the velocities in a given compartment over the number of times (repetitions) that the particle visits that compartment. The turbulence-related correlations can be calculated after the mean velocities are obtained.

Degaleesan's (1997) experiments were performed using air and tap water, at atmospheric pressure. Three columns of internal diameter 0.14, 0.19 and 0.44 m operated at several different superficial gas velocities were studied. Table 1 lists the column diameter, superficial gas velocity, the column's static and dynamic height, and the sparger details.

Computed Tomography (CT) is used to measure time-averaged phase holdup profiles in a vessel, such as gas holdup profiles in a bubble column. By placing a strong gamma-ray source in the plane of interest and a planar array of collimated scintillation detectors on the other side of the reactor, one measures attenuation in the beam of gamma radiation. The attenuation is a function of the line-averaged holdup distribution along the path of the beam. Many such "projections" are obtained at different angular orientations around the reactor. The complete set of projections is then used to back-calculate the cross-sectional distribution of densities. Since the density at any point in the cross-section is a sum of densities of individual phases weighted by their volume fractions, the cross-sectional volume fraction (holdup) distribution of a particular phase can be uniquely recovered provided only two phases are present. The total scanning time is about 2 h, thus the scanned image provides a time-averaged cross-sectional distribution of mixture density. The results for the two-dimensional holdup distribution can be subsequently averaged azimuthally for direct comparison against a suitable axisymmetric simulation.

Details of the experimental setup and the procedures for particle tracking and the tomographic techniques used are available elsewhere (Devanathan et al., 1990; Devanathan, 1991; Moslemian et al., 1992; Y 1992b; Kumar, 1994; Kumar et al., 1995, 1997; Degaleesan, 1997; Roy, 2000).

3. Two-fluid model and population balance

In the present work, the flow in bubble columns was modeled using the Eulerian multiphase model as incorporated in the FLUENT software.

3.1. The Eulerian multiphase model

The governing equations in this approach can be derived by ensemble averaging the fundamental conservation equations for each phase to describe the motion of liquid and gas in a bubble column. Both the continuous and the dispersed phases are modeled in the Eulerian frame of reference as interpenetrating continua. The mass and momentum balance equations are written for each phase separately. The momentum equations of the phases interact with each other through inter-phase momentum exchange terms. The representative contributions to the derivation of this model include studies by Drew (1983), Kashiwa and Rauenzahn (1994), Zhang and Prosperetti (1997) and Drew and Passmann (1999). The continuity equation for each phase is written as

$$\frac{\partial \alpha_k}{\partial t} + \nabla \cdot (\alpha_k \mathbf{u}_k) = 0, \tag{1}$$

where α_k and $\mathbf{u}_k$ are the volume fraction and the phase averaged velocity, respectively, of the liquid phase ($k = l$) and the gas phase ($k = g$). The momentum equation for the liquid phase is

$$\begin{aligned}\frac{\partial(\alpha_k \rho_k \mathbf{u}_k)}{\partial t} &+ \nabla \cdot (\alpha_k \rho_k \mathbf{u}_k \mathbf{u}_k) \\ &= -\alpha_k \nabla P + \alpha_k \rho_k \mathbf{g} \pm \mathbf{F}_{kl} + \nabla \cdot (\alpha_k \boldsymbol{\tau}_k) \\ &\quad + \nabla \cdot (\alpha_k \rho_k \mathbf{u}_k' \mathbf{u}_k'),\end{aligned} \tag{2}$$

where $\mathbf{g}$ is the gravity acceleration, $\mathbf{F}_{kl}$ is the interfacial momentum exchange term, $\boldsymbol{\tau}_k$ is the viscous stress tensor which can be expressed by

$$\boldsymbol{\tau}_k = \mu_k (\nabla \mathbf{u}_k + \nabla \mathbf{u}_k^{\mathrm{T}}) - \frac{2}{3} \mu_k \nabla \cdot \mathbf{u}_k \mathbf{I} \tag{3}$$

Table 1
Column size, sparger design, operating conditions and the corresponding mesh parameters

Column diameter (m)	Superficial gas velocity ($m\,s^{-1}$)	Static liquid height (m)	Dynamic height (m)	Sparger information		$\Delta r (\times 10^{-3}\,m)$	$\Delta z (\times 10^{-3}\,m)$
				Porosity (%)	Size of holes ($\times 10^{-4}\,m$)		
0.14	0.096	0.98	1.23	0.05	4.0	3.7	1.0
0.19	0.02	1.04	1.15	0.05	3.3	5.0	1.0
	0.12	0.96	1.24	0.05	3.3	5.0	1.0
0.44	0.02	1.79	1.93	0.077	7.0	5.0	1.0
	0.10	1.76	2.18	0.077	7.0	5.0	1.0

and $\alpha_k \rho_k \mathbf{u}'_k \mathbf{u}'_k$ is the turbulent stress tensor which needs to be closed by appropriate multiphase turbulence model. Due to the loss of information in the averaging process, several correlations (e.g., the interfacial momentum exchange term, $\mathbf{F}_{kl}$, in Eq. (2)) appear in the macroscopic equations which need to be closed in terms of known variables. In a recent review (Rafique et al., 2004) the various interfacial forces have been discussed. The effect of added mass can be seen only when high frequency fluctuations of the slip velocity occur (Drew, 1983). These high frequency velocity fluctuations (i.e., $\mathbf{u}'_k$), however, are not resolved in the two-fluid model, and are lost in the averaging process. It has been estimated that added mass force are much smaller than the drag force (Oey et al., 2003) in bubbly flow. Even in gas–liquid stirred tank, where the velocity fluctuation is much stronger than in bubble column flows, the inclusion of added mass force has at best a "tuning effect" on the simulation (Jenne, 1999). Mathematically, the inclusion of lift force should have strong effect on the simulation. Oey et al. (2003) estimates that the lift force component in the transversal direction has the same order of magnitude as the corresponding drag force component, provided $C_L = 0.5$, where C_L is the lift force coefficient. However, there are a number of lift forces (e.g. Magnus force, Saffman force, lift force due to bubble deformation, etc.) and there is a dispute regarding the magnitude of the lift force coefficient (Lahey, 1990) and even the sign of the dominant term (Jakobsen et al., 1997). In addition, lift due to bubble deformation is suspected of been dominant in churn turbulent flow and it hasn't yet been modeled properly for inclusion as closure in the Euler–Euler model, and neglecting lift force one can still lead to good comparison with experimental data (Pan et al., 1999, 2000; Pan and Dudukovic, 2001). Subject to these uncertainties, and based on existing evidence that these forces are either smaller compared to drag force or not yet properly modeled, only the drag force is included, while the added mass force and lift force are neglected in the model for inter-phase momentum exchange. Upon completion of our 2D and 3D simulations (in a subsequent paper), we will re-examine the issue of the effect of these forces. The drag force term is calculated by

$$\mathbf{M}_d = \frac{3}{4}\alpha_g \alpha_l \frac{\rho_l}{d_b} C_D |\mathbf{u}_l - \mathbf{u}_g|(\mathbf{u}_l - \mathbf{u}_g). \quad (4)$$

The liquid holdup, α_l, in Eq. (4) accounts for the situation of a bubble moving through a gas–liquid mixture instead of a pure liquid. With this factor, we still use the drag law for a single bubble to approximately calculate the drag coefficient, C_D (Schiller and Naumann, 1933):

$$C_D = \begin{cases} 24\left(\frac{1+0.15Re^{0.687}}{Re}\right) & Re \leqslant 1000, \\ 0.44 & Re > 1000, \end{cases} \quad (5)$$

where $Re = d_b|\mathbf{u}_l - \mathbf{u}_g|\rho_l/\mathbf{u}_l$. By using Eqs. (4) and (5), we attempt to model the bubble–fluid momentum coupling in a very complex system where bubbles of various sizes and shapes exist by assuming that the local mean diameter of the bubbles, which varies with time and position and can be obtained from the population balance equation describes the effect caused by multi-bubble interaction. It should be noted that there are several drag coefficient correlations for gas–liquid system (e.g. Ishii and Zuber, 1979; Tsuchiya et al., 1997) developed from single bubble rising in quiescent liquid or in dilute bubbly flows. However, if they are applied to churn-turbulent flow regime, these correlations significantly overestimate drag coefficient thus one has to artificially increases the bubble size. For example, when Tsuchiya et al.'s (1997) correlation is used to calculate the drag force, the mean bubble size is assigned to 32 mm (from experimentally observed $\sim$ 7 mm) to fit the liquid axial velocity profile in a 0.44 m diameter air–water column operated at $U_g = 0.10$ m/s (Pan and Dudukovic, 2000).

The local bubble diameter is an important needed input parameter for the simulation. In the past it was either estimated from former experience or by a trial-and error method, or it was calculated from available mean bubble diameter correlations. A single value was assigned for whole column in most previous studies except for Krishna and coauthors who uses two bubble classes. In this work we obtain the local mean bubble diameter via the BPBE as discussed in the next section.

Turbulence in the liquid phase is modeled through a set of modified k–ε equations with extra terms that include interphase turbulent momentum transfer (Launder and Spalding, 1974; Elghobashi and Abou-Arab, 1983). For the dispersed gas phase, turbulence closure is effected through correlations from the theory of dispersion of discrete particles by homogeneous turbulence (Tchen, 1947). All of these closures are subject to uncertainties when used in churn-turbulent flow and may need to be improved in the future.

3.2. Bubble Population Balance Equation (BPBE)

In bubble columns, the initial bubble size is determined by the formation of bubbles at the sparger. However, this initial bubble size may not be stable due to turbulence, interfacial instability, wake entrainment, size dependent rise velocity difference and shear layer induced velocity difference. In all these cases, the bubble's size is further determined by a break-up and/or coalescence mechanism. In reaction systems, in addition to the break-up and coalescence, mass transfer should also been considered. Phase change and pressure change may also need to be taken into account.

Since the interfacial area concentration changes with the variation in the bubble number density due to coalescence and break-up, analogous to Boltzmann's transport equation, a population balance model can be used to provide a statistical formulation to describe the dispersed phase in multiphase flow. Generally, the population balance equation can be expressed as

$$\frac{\partial}{\partial t} f(\mathbf{x}, v, t) + \nabla \cdot (\mathbf{u}_b(\mathbf{x}, v, t) f(\mathbf{x}, v, t)) = S(\mathbf{x}, v, t). \quad (6)$$

In this equation $f(\mathbf{x}, v, t)$ is the bubble number density function which is assumed to be continuous and specifies the probable number density of bubbles at a given time t, in the spatial range $\mathrm{d}\vec{x}$ about a position $\vec{x}$, with bubble volumes between v and $v + \mathrm{d}v$. $\mathbf{u}_b(\mathbf{x}, v, t)$ is the local velocity of bubble volumes between v and $v + \mathrm{d}v$ at time t. $S(\mathbf{x}, v, t)$ is the source term which can be expressed as

$$\begin{aligned} S(\mathbf{x}, v, t) &= \tfrac{1}{2}\int_0^v a(v-v', v') f(\mathbf{x}, v-v', t) f(\mathbf{x}, v', t)\,\mathrm{d}v' \\ &\quad - f(\mathbf{x}, v, t)\int_0^\infty a(v, v') f(\mathbf{x}, v', t)\,\mathrm{d}v' \\ &\quad + \int_v^\infty m(v') b(v') P(v, v') f(\mathbf{x}, v', t)\,\mathrm{d}v' \\ &\quad - b(v) f(\mathbf{x}, v, t) + S_{\mathrm{ph}} + S_p + S_r + \cdots, \end{aligned} \tag{7}$$

where the first term is the birth rate of bubbles of volume v due to coalescence of bubbles of volume $v - v'$ and v', the second term is the death rate of bubbles of volume v due to coalescence with other bubbles, the third term is the birth rate of bubbles of volume v due to breakup of bubbles which volume larger than v, and the fourth term is the death rate of bubble of volume v due to breakup. In addition, S_{ph}, S_p and S_r are the bubble source/sink terms due to phase change, pressure change and reaction, respectively; $a(v, v')$ is coalescence frequency between bubbles of volume v and v', $b(v)$ is the breakup frequency of bubbles of volume v, $m(v')$ is the mean number of daughter bubbles produced by breakup of a parent bubble of volume v' and $P(v, v')$ is the p.d.f. of daughter bubbles produced upon breakup of a parent bubble with volume v'. It is clear that the source term needs to be closed by modeling bubble breakup and coalescence.

3.2.1. Breakup closures

Two options are considered in this study. First, the breakup kernel, as given by Luo and Svendsen (1996), for binary breakup is used (Fig. 1a).

$$\Omega_B(v_i : vf_{BV}) = c_B(1-\alpha_g) n_i \left(\frac{\varepsilon}{d^2}\right)^{1/3} \int_{\xi_{\min}}^1 \frac{(1+\xi)^2}{\xi^{11/3}} \times \exp\left(-\frac{12 c_f \sigma}{\beta \rho_c \varepsilon^{2/3} d^{5/3} \xi^{11/3}}\right) \mathrm{d}\xi, \tag{8}$$

where $\Omega_B(v : vf_{BV})$ is the breakup rate per unit volume of the continuous phase ($\mathrm{m^{-3}\,s^{-1}}$) of a parent bubble with volume v into a daughter bubble with volume vf_{BV} (f_{BV} is the volume fraction of the parent bubble that constitutes the volume of one daughter bubble), c_f is defined as the ratio of increased surface area of daughter bubbles with respect to the surface area of parent bubble (i.e., $c_f = f_{BV}^{2/3} + (1 - f_{BV})^{2/3} - 1$), $\xi = \lambda/d$ is the dimensionless eddy size, and λ is the arriving eddy size. This model predicts the breakup rate for bubbles of a given size yielding a prescribed combination of the daughter bubble sizes, and thus does not need a predefined daughter bubble size distribution. The daughter bubble size distribution is a result that arises and can be calculated directly from the model.

As a second option, we considered the phenomenological model (Fig. 1b) for bubble breakup frequency proposed by Martínez-Bazán et al. (1999a). This model is based on the turbulence stress and surface tension force balance and was validated with the authors' experimental data. According to this model,

$$\Omega_B(\varepsilon, d_i) = K_g n_i \frac{\sqrt{\beta(\varepsilon d_i)^{2/3} - 12\sigma/(\rho_c d_i)}}{d_i} \tag{9}$$

where the constant $\beta = 8.2$ was given by Batchelor (1956), and $K_g = 0.25$ was found experimentally by Martínez-Bazán et al. (1999a). The daughter bubble probability density function of (p.d.f.) D^* (D^* is dimensionless diameter of the daughter bubble with respect to parent bubble, $D^* = D/D_0$), $f^*(D^*)$, is given as

$$f^*(D^*) = \frac{\left[D^{*2/3} - \Lambda^{5/3}\right]\left[(1-D^{*3})^{2/9} - \Lambda^{5/3}\right]}{\int_{D^*_{\min}}^{D^*_{\max}} \left[D^{*2/3} - \Lambda^{5/3}\right]\left[(1-D^{*3})^{2/9} - \Lambda^{5/3}\right] \mathrm{d}(D^*)}. \tag{10}$$

Based on Luo and Svendsen's (1996) model, the daughter bubble p.d.f. is U-shaped, while based on Martínez-Bazán et al.'s (1999b) model, the daughter bubble p.d.f. is inverted U- shaped (I-shaped). In this work, we investigated the effect of these quite different breakup closures.

3.2.2. Coalescence closures

The coalescence rates Ω_C ($\mathrm{m^{-3}\,s^{-1}}$) is usually written as the product of collision rate θ_{ij} ($\mathrm{m^{-3}\,s^{-1}}$) and coalescence efficiency P_C (Fig. 2):

$$\Omega_C = \theta_{ij} P_C(d_i, d_j). \tag{11}$$

The collision rate of bubbles per unit volume θ_{ij} ($\mathrm{m^{-3}\,s^{-1}}$), as given by Saffman and Turner (1956), can be written as

$$\theta_{ij} = \frac{\pi}{4} n_i n_j (d_i + d_j)^2 \varepsilon^{1/3} (d_i^{2/3} + d_j^{2/3})^{1/2}. \tag{12}$$

In Eq. (12), d_i, d_j are the diameter of bubbles of class i and j with their number density been given by n_i and n_j, respectively. ε is the turbulent energy dissipation rate per unit volume of liquid. Prince and Blanch (1990) proposed a collision frequency model based on the summation of the turbulent collision rate, buoyancy-driven collision rate and laminar shear collision rate. Only the turbulence collision rate is considered in this work:

$$\theta_{ij} = 0.089\pi n_i n_j (d_{bi} + d_{bj})^2 \varepsilon^{1/3} (d_{bi}^{2/3} + d_{bj}^{2/3})^{1/2}. \tag{13}$$

Several expressions have been proposed for dimensionless coalescence efficiency. Prince and Blanch (1990)

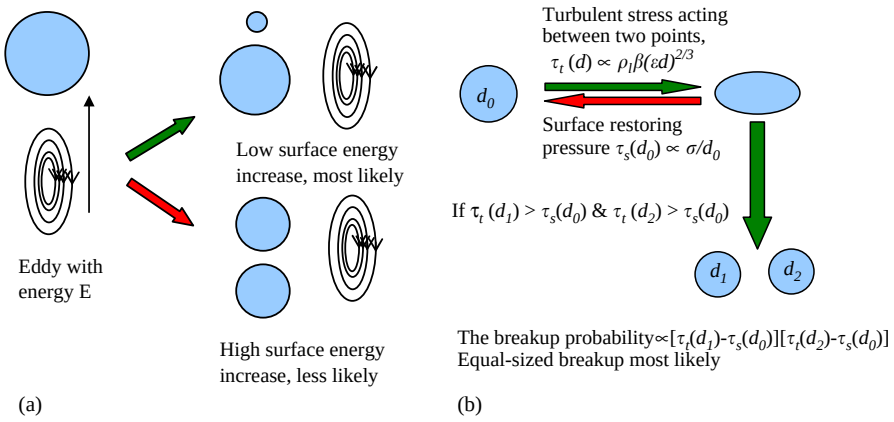

Fig. 1. Breakup model illustration (a) Luo and Svendsen (1996), (b) Martínez-Bazán et al. (1999a,b).

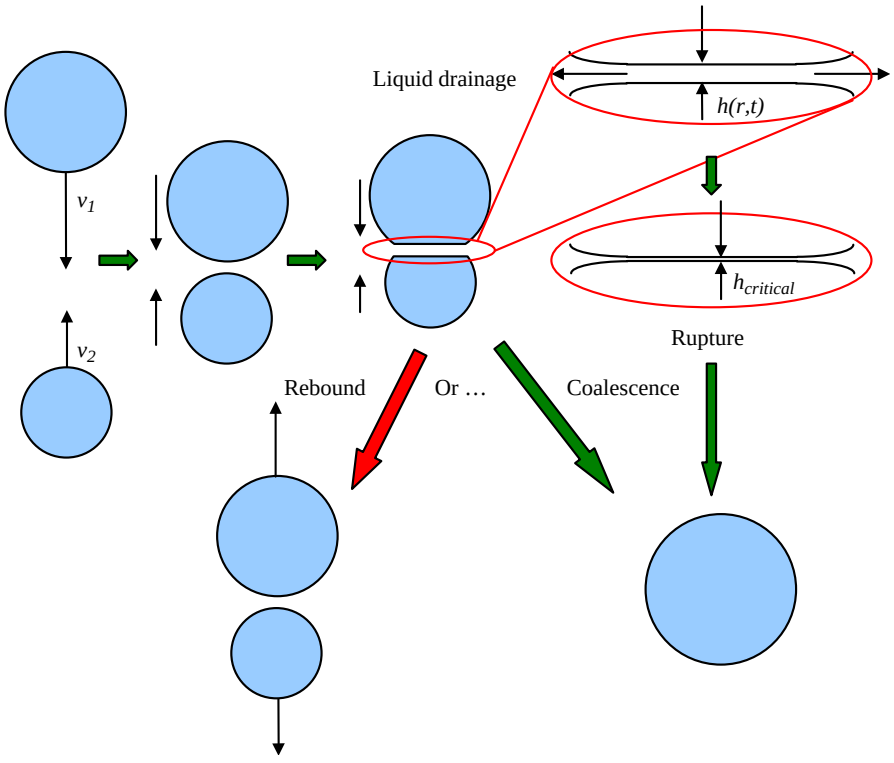

Fig. 2. Bubble coalescence in turbulent flow.

suggested:

$$P_C(r_i, r_j) = \exp\left[-\frac{\left(\frac{r_{ij}^3 \rho_c}{16\sigma}\right)^{1/2} \varepsilon^{1/3} \ln \frac{h_0}{h_f}}{r_{ij}^{2/3}}\right],$$

$$r_{ij} = \left[\frac{1}{2}\left(\frac{1}{r_i} + \frac{1}{r_j}\right)\right]^{-1}, \quad (14)$$

where r_i, r_j are the radius of bubbles of class i and j, h_0, h_f are the initial and critical film thickness between coalescing bubbles. Another expression for the coalescence efficiency (dimensionless) was given by Chesters (1991) as

$$P_C = \exp\left[-c\left(\frac{We}{2}\right)^{1/2}\right], \quad We = \frac{\rho_c(\varepsilon d_{ij})^{2/3} d_{ij}}{2\sigma}, \quad (15)$$

where

$$d_{ij} = \left[\frac{1}{2}\left(\frac{1}{d_i} + \frac{1}{d_j}\right)\right]^{-1}$$

is the equivalent bubble diameter. A third alternative expression for coalescence efficiency (dimensionless) was

proposed by Luo (1993) as

$$P_C(d_i, d_j) = \exp\left\{-c\frac{\left[0.75(1+\xi_{ij}^2)(1+\xi_{ij}^3)\right]^{1/2}}{(\rho_d/\rho_c+0.5)^{1/2}(1+\xi_{ij})^3}\,We_{ij}^{1/2}\right\}, \quad (16)$$

where $We_{ij}=\rho_c d_i \bar{u}_{ij}^2/\sigma$, $\xi_{ij}=d_i/d_j$, $\bar{u}_{ij}=(\bar{u}_i^2+\bar{u}_j^2)^{1/2}=\bar{u}_i(1+\xi_{ij}^{-2/3})$, $\bar{u}_i=\beta^{1/2}(\varepsilon d_i)^{1/2}$.

3.2.3. Solution of the BPBE

There is no analytical solution for Eq. (6) except for a few cases, thus the gas phase needs to be discretized into n subclasses according to bubble size, and be solved separately. Theoretically, one can always solve the continuity and momentum equation of N gas phases (N equals the number of distinct bubble sizes to be tracked) and the liquid phase. However, it is very difficult, if not impossible, to get a large number of highly non-linear momentum equations to converge in a realistic period of time (e.g., $2(N+1)$ equations in 2D and $3(N+1)$ in 3D). To circumvent the problem of solving momentum equations for $N+1$ separate phases, only the continuity and momentum equation for two phases (gas and liquid) is solved as shown below. The population balance equation for the ith bubble class can be written as

$$\frac{\partial}{\partial t}n_i + \nabla\cdot(\mathbf{u}_b n_i) = S_i, \quad (17)$$

where n_i is ith bubble class local number density and $\mathbf{u}_b$ is the local bubble velocity vector. Reaction and phase change are neglected in the present work and the source term due to pressure change is neglected as well. Therefore, the source term S_i is only due to breakup and coalescence of bubbles and its closures will be discussed later. In the present implementation of BPBE in the Euler–Euler model, all the bubbles are assumed to move at identical velocity which equals the local ensemble averaged gas phase velocity, $\mathbf{u}_g$, obtained from the solution of the Euler–Euler model. This avoids solving $N+1$ momentum equation. Bubble–bubble momentum exchange due to collisions is neglected. In addition to local gas velocity $\mathbf{u}_g$, the source term in Eq. (17) also needs local gas holdup and turbulent energy dissipation rate as input, which is obtained from the solution of the Euler–Euler model equation and k–ε model. The assumption that all bubbles travel at the same velocity locally can be questioned as it removes the possibility of bubbles segregating due to different velocities. To test this assumption Chen (2004) implemented the BPBE also in the Algebraic Slip Mixture Model (ASMM). Since only the mixture momentum equation needs now to be solved it is possible to let each bubble class move at the velocity that depends on the size. The results of the ASMM, based on different bubble velocities dependent on size, were compared with the ASMM results based on single bubble velocity independent on size, and were found in excellent agreement. One can hypothesize that the physical explanation for this may be in the fact that in churn turbulent flow at high holdups gas really moves at a prevalent velocity induced by large eddies and is not dependent on bubble size. Hence, single bubble velocity was used in the two-fluid model.

It should be noted that the basic idea, in discretizating the BPBE, is that bubbles in a size range, say R_i, are assigned to a pivotal size x_i. However, breakup and coalescence processes may produce bubbles that are *between* such pivotal sizes (except in the case of a uniform linear grid, i.e., $x_i = i v_{\min}$) and must be reassigned to the pivots (see Fig. 3). The reassignment must be done carefully to preserve the accurate calculation of the selected moments of the p.d.f. of bubble sizes. Kumar and Ramkrishna (1996) proposed the following way to preserve any selected moments. For $x_i \leqslant v < x_{i+1}$, let the fraction of bubbles of size v assigned to x_i be denoted by $\gamma_i^{(i)}$, and a fraction $\gamma_{i+1}^{(i)}$ be assigned to size x_{i+1}. The reassignment will preserve the rth moment provided:

$$\gamma_i^{(i)}(v)x_i^r + \gamma_{i+1}^{(i)}(v)x_{i+1}^r = v^r \quad \text{for } r = r_1, r_2. \quad (18)$$

These two equations above (i.e., Eq. (18) for $r=r_1$ and r_2) yield a unique solution for the quantity $\gamma_i^{(i)}(v)$. In the present work, r was set to 0 and 1 to preserve the mass balance and the number balance, respectively, during the reassignment process. Then, the source term for Eq. (17) may be written as

$$\begin{aligned} S_i(\mathbf{x},t) = & \sum_{x_{i-1}\leqslant(x_j+x_k)\leqslant x_i}^{j\geqslant k} \times\left(1-\frac{1}{2}\delta_{jk}\right)\left[\gamma_i^{(i-1)}(x_j+x_k)a(x_k,x_j)N_jN_k\right] \\ & + \sum_{x_i\leqslant(x_j+x_k)\leqslant x_{i+1}}^{j\geqslant k}\left(1-\frac{1}{2}\delta_{jk}\right) \times\left[\gamma_i^{(i)}(x_j+x_k)a(x_k,x_j)N_jN_k\right] \\ & - N_i\sum_{j=0}^{M}a(x_i,x_j)N_j \\ & + \sum_{j=i}^{M}N_j m(x_j)b(x_j)\pi_{i,j} - b(x_i)N_i, \end{aligned} \quad (19)$$

where $\pi_{i,j} = \int_{x_{i-1}}^{x_i}\gamma_i^{(i-1)}(v)P(v,x_j)\,\mathrm{d}v + \int_{x_i}^{x_{i+1}}\gamma_i^{(i)}(v)P(v,x_j)\,\mathrm{d}v$ and N_i (m^{-3}) is the number density of the ith bubble class.

Eq. (17), which is indeed a scalar transport equation, is solved along with the two-fluid model in a sequential manner to obtain for each bubble class its local number density n_i. The local mean bubble size, which is needed to calculate the drag force, is given as

$$d_b = \frac{\sum_{i=1}^{N}n_i d_i^3}{\sum_{i=1}^{N}n_i d_i^2}. \quad (20)$$

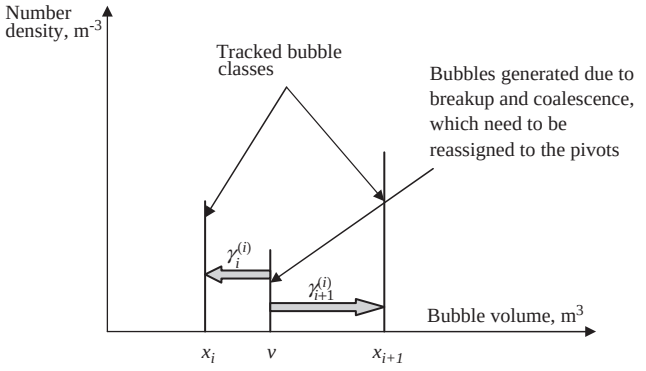

Fig. 3. Bubble reassignment to pivots.

The calculated local mean bubble size, d_b, varies with time and location and is used to calculate the drag force between the two phases.

It should be noted that there are many breakup and coalescence models for liquid–liquid dispersion, which are not applicable for gas–liquid systems. Besides, breakup models that do not specify the daughter bubble p.d.f. cannot be used. In this work, we used pertinent available breakup and coalescence closures for gas–liquid systems.

4. Results and discussion

In order to allow a quantitative comparison with experimental data, we set the conditions for our simulations as those used in the experiments of Kumar (1994), Kumar et al. (1997), Degaleesan (1997), Chen et al. (1999) and Degaleesan et al. (2001). The column size, operating conditions and sparger details, which are needed to calculate initial bubble diameter at the distributor, and the corresponding mesh parameters used for the simulation are listed in Table 1. Initially the column is filled with liquid (water), i.e., $\alpha_l = 1$; $\alpha_g = 0$, up to the level that matches the static liquid height in the experiment. Above this level, the initial condition is $\alpha_l = 0$; $\alpha_g = 1$. To prevent liquid escape from the column (since no net liquid flow is used), the computational domain in the axial direction is about 100% higher than the static liquid height. The gas is introduced at the bottom of the column where only the gas phase is allowed to pass through. Since it is impossible (and it is not necessary) to resolve the gas injectors used in the experiments (e.g., 0.33–0.7 mm diameter holes on the perforated plate) with the currently employed mesh, the gas feed is introduced uniformly over the bottom plane in the simulation. Finally, the pressure condition, i.e., the atmospheric pressure, is imposed on the top of the column.

It is worth noting that the real observed bubble column flows are highly transient and turbulent with rising three-dimensional vortical bubble swarms which cause smaller bubbles and liquid to be trailed in their wakes. The flow never reaches steady-state but time averaging produces reproducable stationary patterns. The axisymmetric boundary condition in 2D computations, however, causes the liquid flow to develop very quickly (5–10 s of real time) and reach its long-time stationary pattern. Thus, in 2D axisymmetric simulation the realizations of the instantaneous hydrodynamic properties cannot be captured, as the instantaneous flow is never axisymmetric in reality, i.e., significant instantaneous azimuthal and radial components do always exist. Besides, the time-scale of the dynamic flows cannot be captured as well. However, the experiments had shown repeatedly (Hills, 1974; Svendsen et al., 1992; Degaleesan, 1997) that, in the time-averaged sense, there is a stationary axisymmetric flow pattern in a cylindrical bubble column. Therefore, it is possible that 2D axisymmetric simulation captures the essence of certain time-averaged hydrodynamic properties in bubble column flows. Since these 2D computations are so much faster to perform, we want to examine to what extent they capture the experimental evidence. Moreover, it is also important to learn the effect of different breakup and coalescence closures before one performs full 3D computations. The breakup and coalescence models implemented in the simulation are listed in Table 2.

Table 2
Implemented breakup and coalescence closures

Case	Breakup closure	Coalescence closure
1	Luo and Svendsen (1996)	Chesters, 1991
2	Luo and Svendsen (1996)	Luo, 1993
3	Martínez-Bazán et al. (1999a,b)	Luo, 1993
4	Luo and Svendsen (1996)	Prince and Blanch, 1990

In churn turbulent flow regime, experimental evidence indicates that there are no significant gas holdup axial gradients in the fully developed flow region (Bukur et al., 1996), which indicates that the breakup and coalescence phenomena are close to equilibrium. This invariance with axial position of radial gas holdup profiles was also experimentally captured by Shollenberger et al. (2000), George et al. (2000) and Ong (2003). In contrast, in our simulations the model predicted coalescence rate is about one order of magnitude higher than the predicted breakup rate calculated from the reported breakup closures. If the coalescence rate is reduced by a factor of 10 in the simulation (i.e., $\Omega_B = \Omega_B^{\text{original}}$, $\Omega_C = 0.1\Omega_C^{\text{original}}$), the simulated mean bubble diameter cannot reach equilibrium in the column. Therefore, breakup rates are enhanced by a factor of 10 (i.e., $\Omega_B = 10.0\Omega_B^{\text{original}}$, $\Omega_C = \Omega_C^{\text{original}}$) in all the simulations. It is important to emphasize that this factor of 10 arose as an engineering estimate and one could obtain "better" comparison against observed data by tweaking this factor. By doing so, however, one loses the predictive nature of CFD, which is one of the main purposes of numerical simulation. Thus, the factor by which breakup rate predicted by reported models is multiplied is fixed at 10 for all the cases studied in this work. One possible reason is the turbulent energy dissipation from the

Table 3
Bubble classes tracked in simulation

Class index	1	2	3	4	5	6	7	8
Bubble diameter ($\times 10^{-3}$ m)	1.00	1.26	1.60	2.00	2.50	3.20	4.00	5.04
Class index	9	10	11	12	13	14	15	16
Bubble diameter ($\times 10^{-3}$ m)	6.35	8.00	10.08	12.70	16.00	20.16	25.40	32.00

turbulence model is not necessarily a physical value (Bertola et al., 2003). A better turbulence model, which properly models the energy containing eddies, is needed in the future.

In our simulation bubbles from 1.0 to 32.0 mm in diameter are divided into 16 classes such that $v_i = 2v_{i-1}$ (see Table 3). The bubble diameter at the sparger (i.e., boundary condition for BPBE) is assumed to be uniform and is calculated from Miyahara et al. (1983) correlation, which can be written as

$$d_s = f(N_w)/(g\rho_l/\sigma d_h)^{1/3}, \tag{21}$$

where

$$\begin{aligned} &f(N_w) = 2.9, && N_w \leqslant 1,\\ &f(N_w) = 2.9N_w^{-0.188}, && 1 < N_w \leqslant 2,\\ &f(N_w) = 1.8N_w^{0.5}, && 2 < N_w \leqslant 4,\\ &f(N_w) = 3.6, && 4 < N_w, \end{aligned}$$

$$N_w = We/Fr^{1/2} = \frac{d_o^{1.5} U_{gh} \rho_l g^{0.5}}{\sigma}.$$

The mean bubble size, assigned to the whole column for all the simulations performed without the BPBE and breakup and coalescence models, is calculated from Wilkinson's (1991) correlation which can be written as

$$d_b = 3g^{-0.44}\sigma^{0.34}\mu_l^{0.22}\rho_l^{-0.45}\rho_g^{-0.11}U_g^{-0.02}. \tag{22}$$

In Fig. 4 the computed time-and-azimuthally averaged liquid axial velocity profiles, $U_z(r)$, are compared against the data obtained by CARPT for the operating conditions reported in Table 1. Different breakup-coalescence closures of Table 2 used in the computation are indicated in the legend of each figure. Wilkinson's (1991) model indicates that single bubble size calculated from his correlation is used throughout the column without BPBE implementation. The compared profiles are for the middle section of the column where the mean flow is usually assumed one-dimensional.

The general shape of the velocity profile is well captured and the discrepancy in the model predicted and CARPT-measured time-averaged axial liquid velocity diminishes as one moves radially outwards in the column. The computed time-averaged liquid velocity from the crossover point to the wall is well predicted while the experimentally observed values in the core region are over-predicted. The observed difference between the data and predicted velocities could be due to the turbulence model (k–ε model) used in the simulation which assumes isotropic unbounded turbulence. Figs. 4b and d illustrate that, with or without BPBE implemented, the simulated liquid velocity profiles are similar in bubbly flow regime where breakup and coalescence phenomena are *not important*. In the churn-turbulent flow regime (Figs. 4a, c, and e) where breakup and coalescence phenomena are *important*, the liquid velocity profiles obtained from simulations with BPBE implemented are closer to the data than those based on an assigned single bubble size obtained from correlation; this is especially true in the core region. However, the effect of different bubble breakup and coalescence models on the simulated liquid velocity profile is insignificant. In all five cases, the simulated centerline liquid velocities are over-predicted which could be due to the nature of the 2D axisymmetric simulation. As mentioned earlier, there are significant instantaneous radial and azimuthal liquid velocity components which cannot be captured in 2D axisymmetric simulation. If the pertinent physics is properly modeled, the actual instantaneous mean energy of the liquid flow, which is acquired from the gas phase (air) due to gas–liquid momentum exchange, and in reality contains contributions from axial, radial and azimuthal velocities, must be the same in 2D axisymmetric simulation which contains only contributions from the axial velocity. This implies that the magnitude of the axial liquid velocity in the 2D axisymmetric simulation has to be over-predicted which is what is seen in all the cases studied.

One may notice that our prediction of the time-averaged liquid axial velocity that is based on the mean bubble size assumption without involving the BPBE is worse than some reported in other studies presented in the open literature. This is due to the fact that our computation that uses the mean bubble size assumption in this work remains predictive as the bubble diameter used as input is calculated from Wilkinson's (1991) correlation and is not selected to fit the data better. In fact, one may "tweak" the input bubble diameter to obtain a "better" fit, as illustrated in Fig. 5. The mean bubble diameter used in Fig. 5 is 8.5 mm. In the literature it is not always clear whether the mean bubble size used or the simulation was based on independent experimental evidence or was adjusted to fit the data.

In Fig. 6 the computed time-and-azimuthally averaged liquid kinetic energy (obtained by solution of the k–ε model in the simulations) profiles are compared against data obtained by CARPT. In churn-turbulent flow regime (Figs. 6a, c and e), kinetic energy profiles typically exhibit a maximum around the cross-over point for the time-averaged liquid axial velocity, due to large gradients and large fluctuations

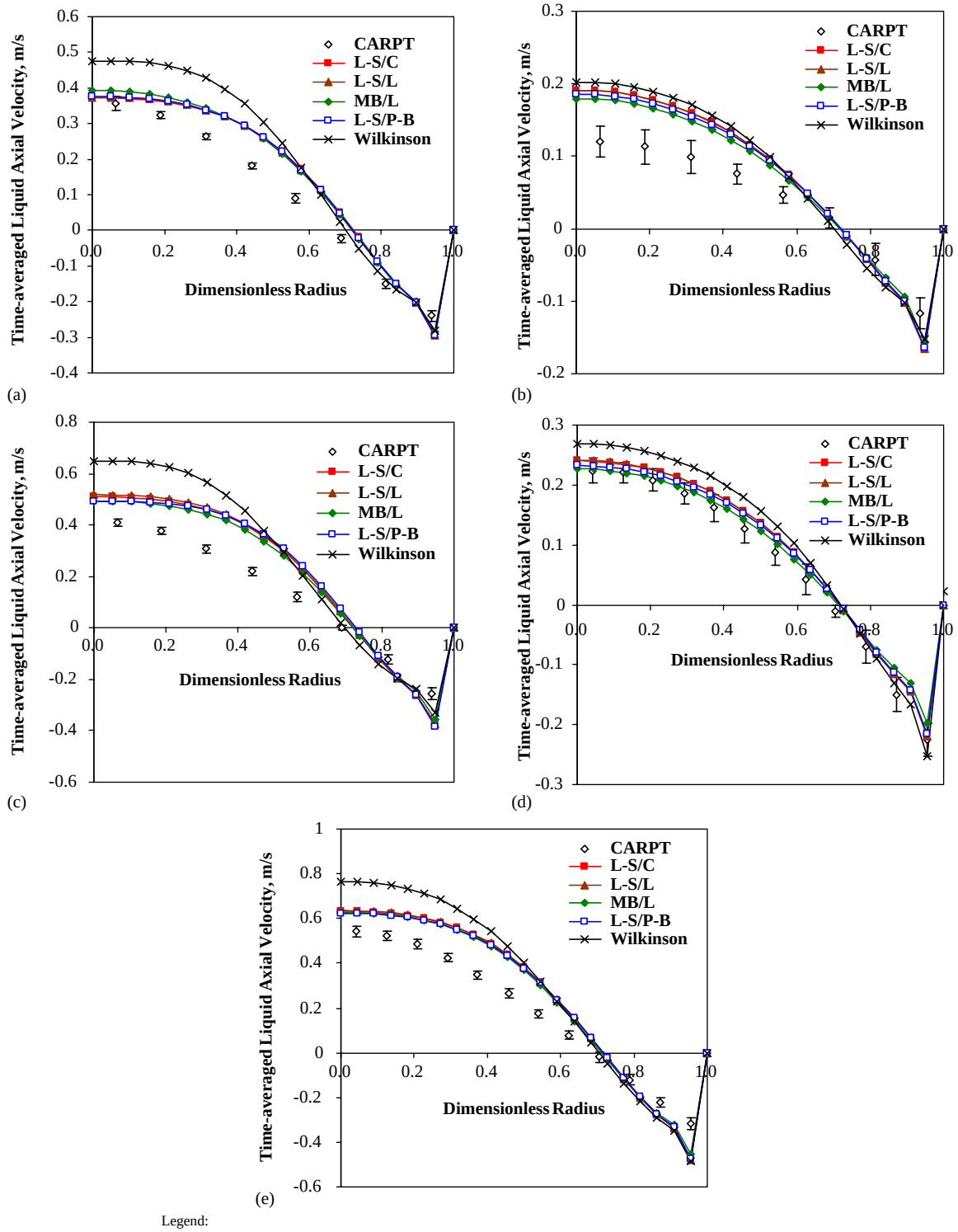

Legend:

CARPT	Experimental data obtained via CARPT	
L-S/C	Luo and Svendsen, 1996 (Breakup)	Chesters, 1991 (Coalescence)
L-S/L	Luo and Svendsen, 1996 (Breakup)	Luo, 1993 (Coalescence)
MB/L	Martínez-Bazán et al., 1999a; b (Breakup)	Luo, 1993 (Coalescence)
L-S/P-	B Luo and Svendsen, 1996 (Breakup)	Prince and Blanch, 1990 (Coalescence)
Wilkinson	Wilkinson, 1991 (Bubble Mean Diameter Correlation)	

Fig. 4. Comparison of the radial profiles of the axial liquid velocity obtained from simulations with experimental data (Degaleesan, 1997) measured by CARPT for (a) 0.14 m diameter column operated at $U_g = 0.096\,\mathrm{m\,s^{-1}}$; (b) 0.19 m diameter column operated at $U_g = 0.02\,\mathrm{m\,s^{-1}}$; (c) 0.19 m diameter column operated at $U_g = 0.12\,\mathrm{m\,s^{-1}}$; (d) 0.44 m diameter column operated at $U_g = 0.02\,\mathrm{m\,s^{-1}}$; (e) 0.44 m diameter column operated at $U_g = 0.10\,\mathrm{m\,s^{-1}}$.

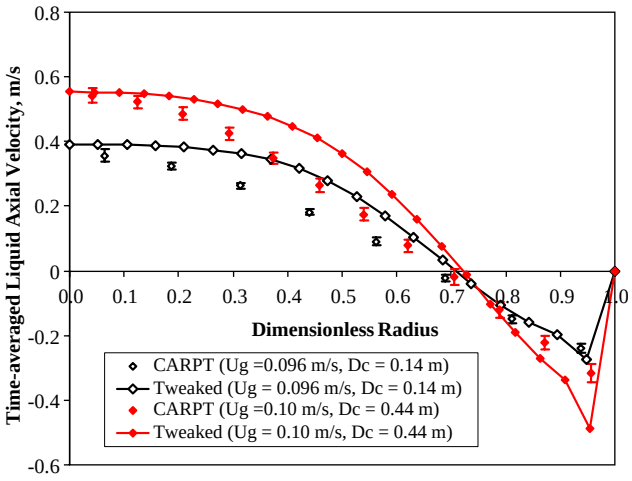

Fig. 5. Comparison of the radial profiles of the axial liquid velocity obtained from simulations by "tweaked" mean bubble size with experimental data (Degaleesan, 1997) measured by CARPT.

in the liquid velocity. In the bubbly regime this effect is not very significant (because of suppressed turbulence) and the liquid turbulent kinetic energy is practically flat as a function of radius. These effects are clearly captured in the simulation results presented in Figs. 6b and d. For all the cases, the simulations with BPBE implemented give better prediction of data especially in the churn-turbulent flow regime. The impact of different breakup and coalescence closures is again not significant for turbulent kinetic energy prediction. Turbulent kinetic energy obtained from the two-phase k–ε formulation arises from the turbulence microscale, while that obtained from experiments like CARPT arises from the larger scales. (For example, it is estimated that the "CARPT tracer particle" cannot respond to the turbulence fluctuations above 20–25 Hz in frequency.) It seems that a meaningful comparison of kinetic energy cannot be made as they are not of the same scale. However, as illustrated by Sanyal et al. (1999), in the present type of axisymmetric simulations, the "turbulent" kinetic energy (i.e., all the flow energy that is not due to the mean flow) is forced to represent the large scale turbulent kinetic energy as measured by CARPT. In other words, the 2D axisymmetric simulation indicates all the turbulence time scales smaller than the total averaging time to contribute to the turbulent kinetic energy at the "microscale" (hence, captured by the k–ε model). One also should expect a reasonable comparison of the overall kinetic energy profiles if the mean velocity profile and gas holdup profile are reasonably predicted.

In Fig. 7 the typical time-and-azimuthally averaged gas holdup profiles in churn turbulent flow regime computed based on various closures of Table 2 are compared. In Fig. 7, comparison of the simulation with data obtained by Computed Tomography (CT). This also shows the assumption of cylindrical axisymmetry in the computation prevents lateral motion of the dispersed gas phase and leads to an unrealistic gas holdup distribution wherein a maximum holdup is away from the centerline, which is also reported by other authors (e.g. Krishna et al., 2000). In order to get rid of this "hump" profile, full three-dimensional simulation is necessary to obtain more realistic radial gas holdup profiles as will be shown in a subsequent communication. The predicted gas holdup obtained from constant mean bubble size simulation is higher in the core region and lower in the wall region than that obtained from simulation with BPBE implemented. One of the reasons could be due to the fact that the local mean bubble size in the core region is larger than in the wall region, which is captured by BPBE, as illustrated in Figs. 8a and b. In the core region of the bubble column, gas holdup is higher, while dissipation rate is lower, which results in larger bubbles because of the higher coalescence rate and lower breakup rate. On the other hand, gas holdup is lower while dissipation rate is higher in the wall region, which results in smaller bubbles because of the lower coalescence rate and higher breakup rate. Although the effects of breakup and coalescence closures on the predicted gas holdup, liquid axial velocity and kinetic energy are not significant, their effect on the predicted Sauter mean bubble size is apparent (see Fig. 8b). In Fig. 9, the effect of breakup and coalescence closure on the bubble volume-based p.d.f. is illustrated. It can be seen that the effect of these drastically different breakup models (Luo and Svendsen, 1996; Martínez-Bazán et al., 1999a,b) are substantial. Martínez-Bazán et al.'s (1999a,b) model produces significantly fewer smallest bubbles and more largest bubbles, and the bubble size distribution is significantly narrower as compared to the one when Luo and Svendsen's (1996) model is applied. Rigorous local experiments are needed in order to test these available breakup and coalescence closures.

In Figs. 10a and b the computed time averaged interfacial area density is displayed. The effect of BPBE on the computed interfacial area density, which is of great interest in bubble column industrial operation, is significant ($\sim$ 100% difference). Uniformately, there is no experimental data available at present for the interfacial area density distribution. The significant difference between the simulated interfacial area results mentioned earlier suggests that BPBE may be necessary when gas–liquid transfer needs to be considered.

One would expect that without well-predicted gas holdup profile, the bubble size distribution profile and Sauter mean bubble diameter cannot be accurately predicted because gas holdup is needed in the breakup and coalescence closures. However, qualitative conclusions may still be possible. In Fig. 11 the computed evolution of the local Sauter mean bubble diameter along the centerline of the column is illustrated. In churn turbulent flow regime, the Sauter mean bubble diameters are stabilized after 1–2 column diameters as the breakup and coalescence reach equilibrium, while this is not the case in bubbly flow. Moreover, it seems that the coalescence rates are over-predicted in the bubbly flow regime. This is expected because the bubble net birth rate is roughly

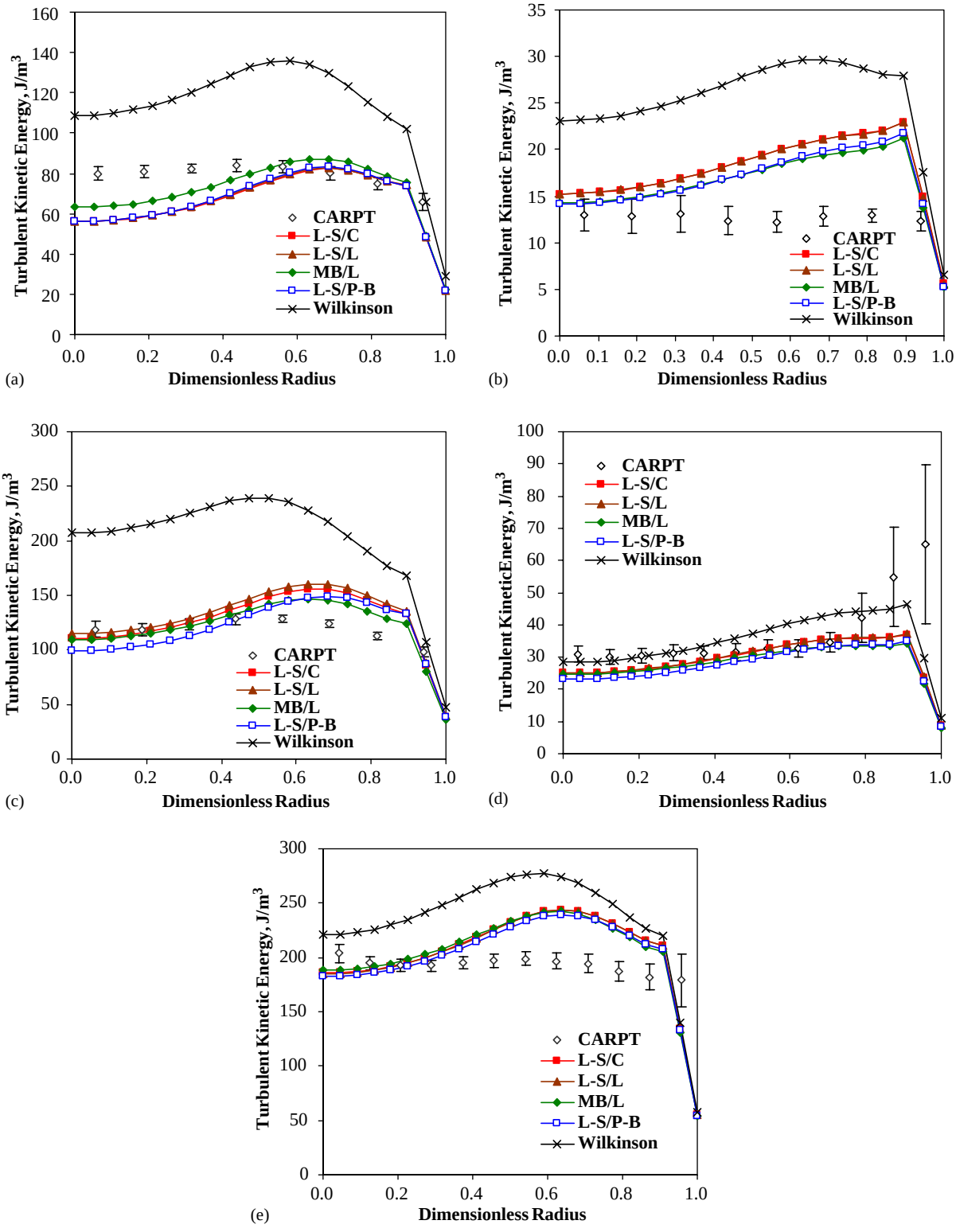

Fig. 6. Comparison of the radial profiles of the kinetic energy obtained from simulations with experimental data measured by (Degaleesan, 1997) CARPT for (a) 0.14 m diameter column operated at $U_g = 0.096\,\mathrm{m\,s^{-1}}$; (b) 0.19 m diameter column operated at $U_g = 0.02\,\mathrm{m\,s^{-1}}$; (c) 0.19 m diameter column operated at $U_g = 0.12\,\mathrm{m\,s^{-1}}$; (d) 0.44 m diameter column operated at $U_g = 0.02\,\mathrm{m\,s^{-1}}$; (e) 0.44 m diameter column operated at $U_g = 0.10\,\mathrm{m\,s^{-1}}$.

proportional to $-K_1\alpha_g\varepsilon^{1/3} + K_2\varepsilon^{1/3}\exp(-K_3\varepsilon^{1/3})\alpha_g$ according to the current breakup and coalescence models used in this work. The exponential dependence of the coalescence rate (i.e., $K_2\varepsilon^{1/3}\exp(-K_3\varepsilon^{1/3})\alpha_g$) on the local turbulent dissipation rate leads to coalescence dominating the bubbly flow simulation. However, the used breakup and coalescence

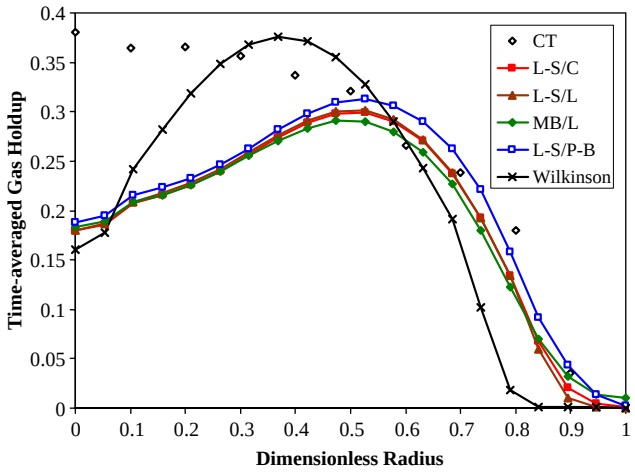

Fig. 7. Comparison of the radial profiles of the gas holdup obtained from simulations with experimental data (Kumar, 1994) measured by CT for a 0.19 m diameter column operated at $U_g = 0.12\,\mathrm{m\,s^{-1}}$.

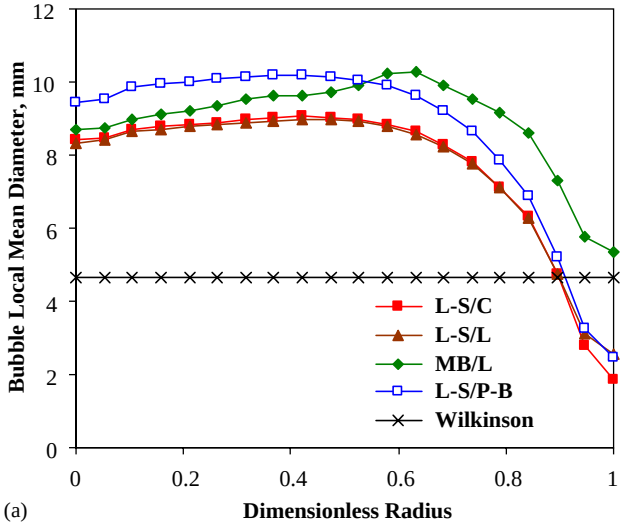

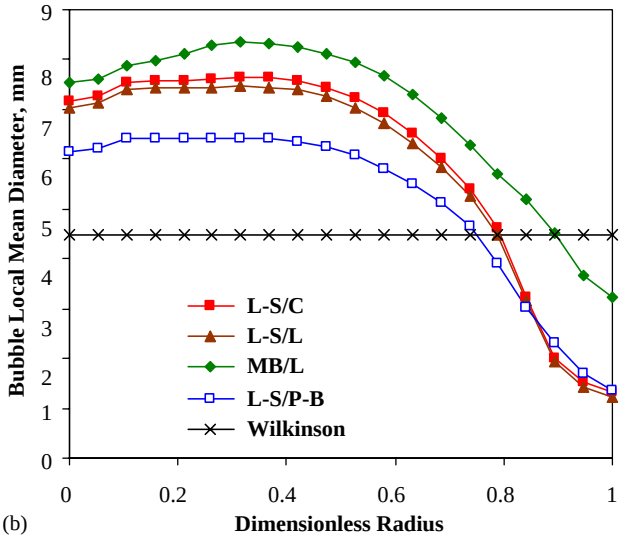

Fig. 8. Comparison of the radial profiles of the bubble local mean diameter for 0.19 m diameter column operated at (a) $U_g = 0.02\,\mathrm{m\,s^{-1}}$; (b) $U_g = 0.12\,\mathrm{m\,s^{-1}}$.

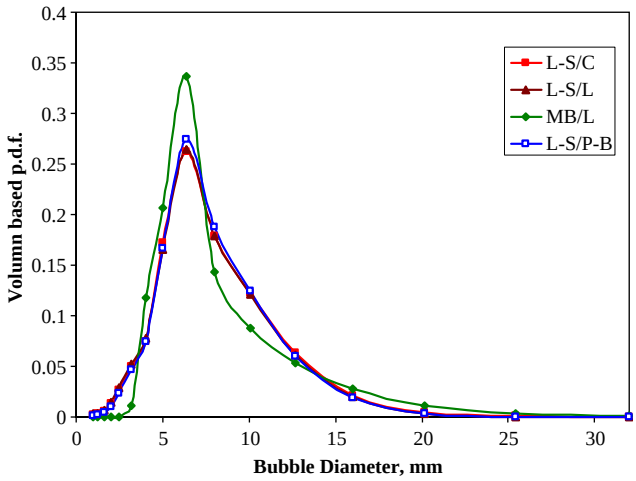

Fig. 9. Comparison of the bubble volume-based p.d.f. for a 0.44 m diameter column operated at $U_g = 0.10\,\mathrm{m\,s^{-1}}$.

models are developed based on bubbles immersed in a highly turbulent field which may not be applicable in bubbly flow. It seems that improved breakup and coalescence closures both in bubbly flow regime and churn-turbulent flow are needed for different reasons (under-prediction of breakup in churn-turbulent flow and over- prediction of coalescence in bubbly flow). On the other hand, as illustrated earlier, one may not need to implement BPBE in the bubbly flow regime simulation at all as the bubble size distribution is narrow and all that is needed is the prediction of mean bubble size.

In Figs. 12a and b, the evolution of cross-sectional bubble class volume based p.d.f. is presented. For churn-turbulent flow ($U_g = 0.096$ and 0.10 m/s), the bubble class distribution stabilized after 1.5–3 column diameter. It seems that the bubble size distribution in bigger diameter column needs more height to reach a stable profile (0.60 in 0.44 m diameter column and 0.40 in 0.14 m diameter column for U_g about $0.10\,\mathrm{m\,s^{-1}}$), however, the effect is not significant.

5. Conclusions

Reasonable agreement was obtained between the experimental data and two-dimensional axisymmetric simulations for the time-averaged axial liquid velocity profiles, as well as for the kinetic energy profiles. It is found that the model predicted coalescence rate and breakup rate are out of balance by an order of magnitude (the former being the larger). To match experimental evidence the breakup rate was increased by a factor of 10. The unrealistic time-averaged gas holdup profiles arise due to the nature of two-dimensional axisymmetric simulations and suggest that full three-dimensional simulation is needed. Better agreement with data is obtained with the BPBE implemented, especially in the churn-turbulent flow regime, compared with the simulation using a constant mean bubble size. The difference in predicted

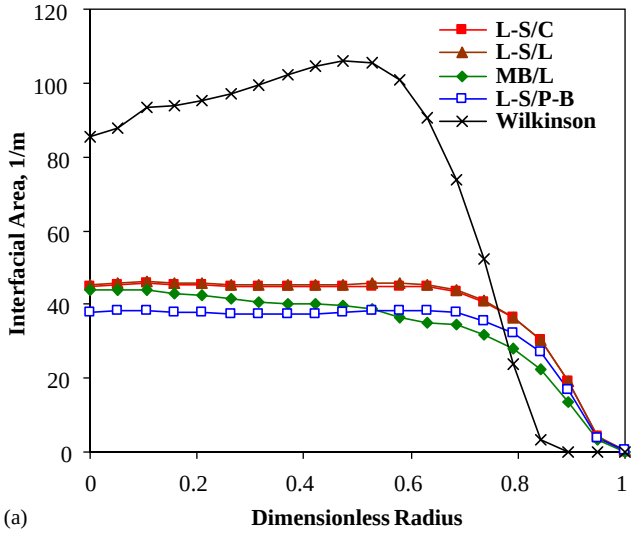

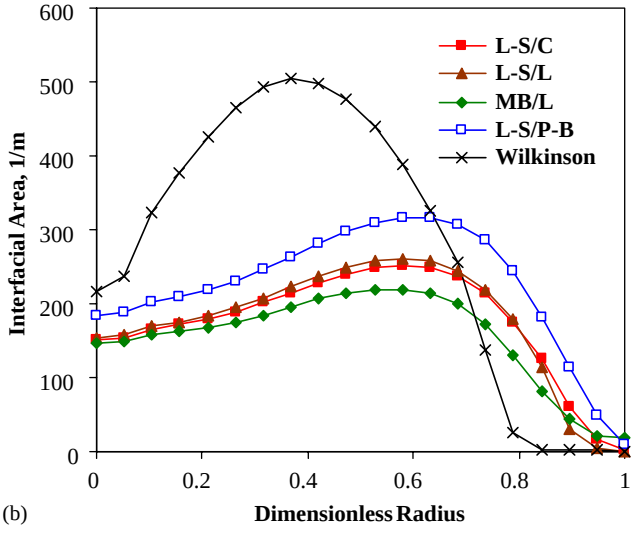

Fig. 10. Comparison of the radial profiles of the interfacial area for 0.19 m diameter column operated at (a) $U_g = 0.02\,\mathrm{m\,s^{-1}}$; (b) $U_g = 0.12\,\mathrm{m\,s^{-1}}$.

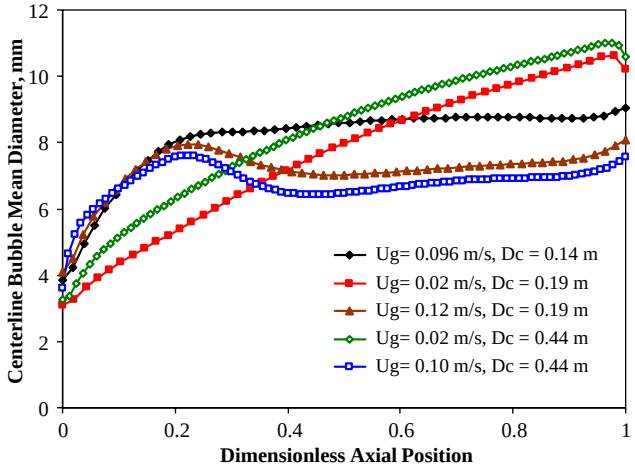

Fig. 11. Centerline mean bubble diameter evolution.

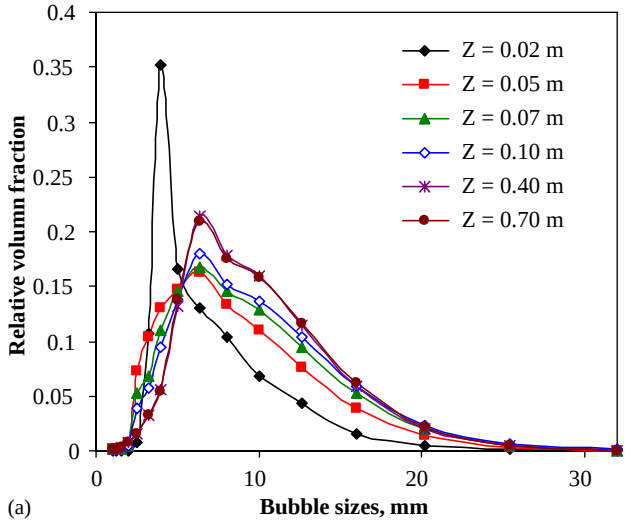

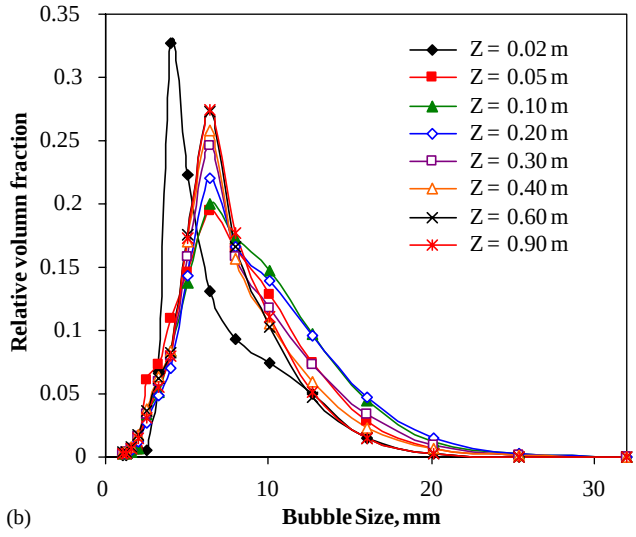

Fig. 12. Bubble size distribution evolution along column elevation in (a) 0.14 m diameter column operated at $U_g = 0.096\,\mathrm{m\,s^{-1}}$; (b) 0.44 m diameter column operated at $U_g = 0.10\,\mathrm{m\,s^{-1}}$.

interfacial area densities, with and without BPBE implemented, is significant. The choice of current available bubble breakup and coalescence closures does not have significant impact on the simulated results. However, implementation of BPBE is necessary for churn-turbulent flow simulation when interfacial area density information is important.

Notation

a	breakup frequency, $\mathrm{s^{-1}}$
b	coalescence frequency, $\mathrm{s^{-1}}$
c	dimensionless constant in Eqs. (15) and (16), $c = 0.4$
c_B	dimensionless constant in Eq. (8), $c \approx 0.923$

c_f	coefficient of surface area increase, $c_f = f_{BV}^{2/3} + (1 - f_{BV})^{2/3} - 1$
C_D	drag coefficient, dimensionless
d, d_B	bubble diameter, m
d_h	sparger orifice diameter, m
d_s	bubble diameter at the sparger, m
D^*	dimensionless daughter bubble diameter, $D^* = D/D_0$
$D^*_{\max}$	maximum dimensionless daughter bubble diameter, $D^*_{\max} = [1 - (D_{\min}/D_0)^3]^{1/3}$
$D^*_{\min}$	minimum dimensionless daughter bubble diameter, $D^*_{\min} = (12\sigma/(\beta\rho_l))^{3/2} D_0^{-5/2} \varepsilon^{-1}$
f	bubble number density function
f^*	daughter bubble p.d.f. function
f_{BV}	volume fraction of parent bubble in one daughter bubble, dimensionless
$\mathbf{F}_{kl}$	interfacial momentum exchange term, $\mathrm{N\,m^{-3}}$
$\mathbf{g}$	gravity, $\mathrm{m^2\,s^{-1}}$
h	film thickness between coalescing bubbles, m
K_g	dimensionless constant in Eq. (9)
m	mean number of daughter bubbles produced by breakup, dimensionless
$\mathbf{M}_d$	drag force per unit volume, $\mathrm{N\,m^{-3}}$
n, N	number density of bubble class, $\mathrm{m^{-3}}$
N_w	in Eq. (21),$N_w = We/Fr^{1/2} = \frac{d_o^{1.5} U_{gh} \rho_l g^{0.5}}{\sigma}$
P	pressure, Pa
P_C	coalescence efficiency, dimensionless
P_d	daughter bubble p.d.f.
r	bubble radius, m
Re	local bubble Reynolds number, dimensionless, $Re = d_b \lvert\mathbf{u}_l - \mathbf{u}_g\rvert \rho_l/\mu_l$
S	source term, $\mathrm{s^{-1}}$
S_i	source term, $\mathrm{m^{-3}\,s^{-1}}$
$\bar{u}_i, \bar{u}_j$	bubble turbulent velocity, $\mathrm{m\,s^{-1}}$
$\bar{u}_{ij}$	bubble approaching turbulent velocity, $\mathrm{m\,s^{-1}}$
$\mathbf{u}$	velocity, $\mathrm{m\,s^{-1}}$
$\mathbf{u}'$	velocity fluctuation, $\mathrm{m\,s^{-1}}$
v, v'	bubble volume, $\mathrm{m^3}$
U_g	superficial gas velocity, $\mathrm{m\,s^{-1}}$
U_{gh}	gas velocity at the sparger holes, $\mathrm{m\,s^{-1}}$
t	time, s
$3We$	Webber number, dimensionless, $We = \frac{\rho_c (\varepsilon d)^{2/3} d}{2\sigma}$
$\mathbf{x}$	position vector
x_i	diameter of ith bubble tracked in BPBE, m

Greek letters

α	void fraction, dimensionless
β	dimensionless constant in Eqs. (8) and (9)
γ	fraction to be reassigned to nearby bubble classes, dimensionless
ε	turbulence energy dissipation rate, $\mathrm{m^2\,s^{-3}}$
θ	collision rate, $\mathrm{m^{-3}\,s^{-1}}$
λ	arriving eddy size, m
Λ	dimensionless critical diameter, $\Lambda = D_c/D_0 = (12\sigma/(\beta\rho_l))^{3/5} \varepsilon^{-2/5} D_0^{-1}$
μ	dynamic viscosity, $\mathrm{kg\,m^{-1}\,s^{-1}}$
ξ	d_i/d_j or λ/d, dimensionless
$\pi_{i,j}$	defined in Eq. (19)
ρ	density, $\mathrm{kg\,m^{-3}}$
σ	surface tension, $\mathrm{N\,m^{-1}}$
τ	shear stress tensor, Pa
Ω_B	breakup rate, $\mathrm{m^{-3}\,s^{-1}}$

Subscripts

b	bubble
c	continuous phase
d	dispersed phase
g	gas phase index
i, j	bubble class
k	phase index
l	liquid phase
p	particle

Superscripts

i	bubble class index
p	pressure change
ph	phase change
r	reaction
T	turbulence

Acknowledgements

Two of the authors (P. Chen and M.P. Duduković) acknowledge the support of Air Products via contract from the Department of Energy (DE-FG22-95PC95051). We express our sincere appreciation to Dr. S. Vasquez of Fluent, Inc. for formulating the original multiphase model in Fluent v6.

References

Batchelor, G.K., 1956. The Theory of Homogeneous Turbulence, Cambridge University Press, Cambridge.

Bertola, F., Grundseth, J., Hagesaether, L., Dorao, C., Luo, H., Hjarbo, K.W., Svendsen, H.F., Vanni, M.B., Jakobsen, H.A., 2003. Numerical analysis and experimental validation of bubble size distributions in two phase bubble column reactors. 3rd European-Japanese Two-Phase Flow Group Meeting, Certosa di Pontignano.

Bukur, D.B., Daly, J.G., Patel, S.A., 1996. Application of γ-ray attenuation for measurement of gas holdups and flow regime transitions in bubble columns. Industrial & Engineering Chemistry Research 35, 70.

Bunner, B., Tryggvason, G., 1999. Direct numerical simulations of three-dimensional bubbly flows. Physics of Fluids 11, 1967–1969.

Chen, P., 2004. Fluid dynamic modeling of bubble column flows. D.Sc. Thesis, Washington University, Saint Louis, MO.

Chen, J., Li, F., Degaleesan, S., Gupta, P., Al-Dahhan, M.H., Dudukovic, M.P., Toseland, B.A., 1999. Fluid dynamic parameters in bubble columns with internals. Chemical Engineering Science 54, 2187–2197.

Chesters, A.K., 1991. The modeling of coalescence processes in fluid–liquid dispersions. Transactions of the Institution of Chemical Engineers 69, 259–270.

Degaleesan, S., 1997. Fluid dynamic measurements and modeling of liquid mixing in bubble columns. D.Sc. Thesis, Washington University, St. Louis.

Degaleesan, S., Dudukovic, M.P., Pan, Y., 2001. Experimental study of gas-induced liquid-flow structures in bubble columns. A.I.Ch.E. Journal 47, 1913–1931.

Delnoij, E., Lammers, F.A., Kuipers, J.A.M., van Swaaij, W.P.M., 1997. Dynamic simulation of dispersed gas–liquid two-phase flow using a discrete bubble model. Chemical Engineering Science 52, 1429–1458.

Devanathan, N., 1991. Investigation of liquid hydrodynamics in bubble columns via computer automated radioactive particle tracking (CARPT). D.Sc. Thesis, Washington University, St. Louis.

Devanathan, N., Moslemian, D., Dudukovic, M.P., 1990. Flow mapping in bubble columns using CARPT. Chemical Engineering Science 45, 2285–2291.

Drew, D.A., 1983. Mathematical modeling of two-phase flow. Annual Review of Fluid Mechanics 15, 261–291.

Drew, D.A., Passmann, S.L., 1999. Theory of Multicomponent Fluids, Springer, New York.

Druzhinin, O.A., Elghobashi, S., 1998. Direct numerical simulations of bubble-laden turbulent flows using the two-fluid formulation. Physics of Fluids 10, 685–697.

Dudukovic, M.P., Degaleesan, S., Gupta, P., Kumar, S.B., 1997. Fluid dynamics in churn-turbulent bubble columns: measurements and modeling. 1997 ASME Fluid Engineering Division Summer Meeting.

Elghobashi, S.E., Abou-Arab, T.W., 1983. A two-equation turbulence model for two-phase flows. Physics of Fluids 26, 931–938.

George, D.L., Shollenberger, K.A., Torczynski, J.R., 2000. Sparger effect on gas volume fraction distributions in vertical bubble-column flows as measured by gamma-densitometry tomography. ASME 2000 Fluids Engineering Division Summer Meeting, Boston, MA.

Hills, J.H., 1974. Radial non-uniformity of velocity and voidage in a bubble column. Transactions of Institution of Chemical Engineers 52, 1–9.

Ishii, M., Zuber, N., 1979. Drag coefficient and relative velocity in bubbly, droplet or particulate flows. A.I.Ch.E. Journal 25, 843–855.

Jakobsen, H.A., Sannaes, B.H., Grevskott, S., Svendsen, H., 1997. Modelling of vertical bubble-driven flows. Industrial & Engineering Chemistry Research 36, 4052–4074.

Jenne, M., 1999. Modellierung und Simulation der Strömungsverhältnisse in begasten Rührkesselreaktoren. D.Sc. Thesis, Universität Stuttgart.

Joseph, D.D., 2002. Interrogations of direct numerical simulation of solid–liquid flow, www.eFluids.com.

Kashiwa, B.A., Rauenzahn, R.M., 1994. A multimaterial formalism. FED (American Society of Mechanical Engineers) 185, 149–157.

Krishna, R., Ellenberger, J., Sie, S.T., 1996. Reactor development for conversion of natural gas to liquid fuels: a scale-up strategy relying on hydrodynamic analogies. Chemical Engineering Science 51, 2041–2050.

Krishna, R., van Baten, J.M., Urseanu, M.I., 2000. Three-phase Eulerian simulations of bubble column reactors operating in the churn-turbulent regime: a scale up strategy. Chemical Engineering Science 55, 3275–3286.

Kumar, S.B., 1994. Computed tomographic measurements of void fraction and modeling of the flow in bubble columns. D.Sc. Thesis, Florida Atlantic University, Boca Raton, FL, USA.

Kumar, S., Ramkrishna, D., 1996. On the solution of population balance equations by discretization—I. A fixed pivot technique. Chemical Engineering Science 51, 1311.

Kumar, S.B., Moslemian, D., Dudukovic, M.P., 1995. A gamma-ray tomographic scanner for imaging voidage distribution in two-phase flow systems. Flow Measurement and Instrumentation 6, 61–73.

Kumar, S.B., Moslemian, D., Dudukovic, M.P., 1997. Gas-holdup measurements in bubble columns using computed tomography. A.I.Ch.E. Journal 43, 1414–1425.

Lahey, R.T., 1990. The analysis of phase separation and phase distribution phenomena using two-fluid model. Advances in Nuclear Engineering and Design 122, 17.

Lahey Jr., R.T., Drew, D.A., 2001. The analysis of two-phase flow and heat transfer using a multidimensional, four field, two-fluid model. Nuclear Engineering and Design 204, 29–44.

Lapin, A., Lübbert, A., 1994. Numerical simulations of the dynamics of two-phase gas–liquid flows in bubble columns. Chemical Engineering Science 49, 3661–3674.

Launder, B.E., Spalding, D.B., 1974. Mathematical Models of Turbulence, Academic Press, London.

Luo, H., 1993. Coalescence, breakup and liquid circulation in bubble column reactors. D.Sc. Thesis, Norwegian Institute of Technology.

Luo, H., Svendsen, H.F., 1996. Theoretical model for drop and bubble breakup in turbulent dispersions. A.I.Ch.E. Journal 42, 1225–1233.

Martínez-Bazán, C., Montañéz, J.L., Lasheras, J.C., 1999a. On the breakup of an air bubble injected into a fully developed turbulent flow. Part 1: breakup frequency. Journal of Fluid Mechanics 401, 157.

Martínez-Bazán, C., Montañéz, J.L., Lasheras, J.C., 1999b. On the breakup of an air bubble injected into a fully developed turbulent flow. Part 2: size PDF of the resulting daughter bubbles. Journal of Fluid Mechanics 401, 183.

Miyahara, T., Matsuba, Y., Takahashi, T., 1983. The size of bubbles generated from perforated plates. International Chemical Engineering 23, 517.

Moslemian, D., Devanathan, N., Dudukovic, M.P., 1992. Radioactive particle tracking technique for investigation of phase recirculation and turbulence in multiphase systems. Review of Scientific Instruments 63, 4361–4372.

Oey, R.S., Mudde, R.F., Van den Akker, H.E.A., 2003. Sensitivity study on interfacial closure laws in two-fluid bubbly flow simulations. A.I.Ch.E. Journal 49, 1621–1636.

Ong, B., 2003. Experimental investigation of bubble column hydrodynamics—effect of elevated pressure and superficial gas velocity. D.Sc. Thesis, Washington University, Saint Louis, USA.

Pan, Y., Dudukovic, M.P., 2000. Mean Axial Liquid Velocity Profiles in Bubble Columns—Numerical versus CARPT. CREL Annual Meeting.

Pan, Y., Dudukovic, M.P., 2001. CFD simulations of a bubble column—2D versus 3D. 6th World Congress of Chemical Engineering, Melbourne, Australia.

Pan, Y., Dudukovic, M.P., Chang, M., 1999. Dynamic simulation of bubbly flow in bubble columns. Chemical Engineering Science 54, 2481–2489.

Pan, Y., Dudukovic, M.P., Chang, M., 2000. Numerical investigation of gas-driven flow in 2-D bubble columns. A.I.Ch.E. Journal 46, 434–449.

Prince, M.J., Blanch, H.W., 1990. Bubble coalescence and break-up in air-sparged bubble columns. A.I.Ch.E. Journal 36, 1485.

Rafique, M., Chen, P., Dudukovic, M., 2004. Computational modeling of gas–liquid flow in bubble columns. Reviews in Chemical Engineering 20(3–4), 225–375.

Roy, S. 2000. Quantification of two-phase flow in liquid–solid risers. D.Sc. Thesis, Washington University, Saint Louis.

Saffman, P.G., Turner, J.S., 1956. On the collision of drops in turbulent clouds. Journal of Fluid Mechanics 1, 16.

Sanyal, J., Vasques, S., Roy, S., Dudukovic, M.P., 1999. Numerical simulations of gas–liquid dynamics in cylindrical bubble column reactors. Chemical Engineering Science 54, 5071–5084.

Schiller, L., Naumann, Z., 1933. Über die grundlegenden Berechungen bei der Schwerkraftaufbereitung. Zeitschrift des Vereiner der Deutscheutschen Ingenieur 77, 318.

Shah, Y.T., Kelkar, B.G., Godbole, S.P., Deckwert, W.D., 1982. Design parameters estimations for bubble column reactor. A.I.Ch.E. Journal 28, 353–379.

Shollenberger, K.A., George, D.L., Torczynski, J.R., 2000. Effect of sparger geometry on gas-volume-fraction in bubble-column flows measured by gamma-densitometry tomography (GDT). Sandia National Laboratories.

Sokolichin, A., Eigenberger, G., 1994. Gas–liquid flow in bubble columns and loop reactors: Part I. Detailed modelling and numerical simulation. Chemical Engineering Science 49, 5735–5746.

Svendsen, H.F., Jakobsen, H.A., Torvik, R., 1992. Local flow structure in internal loop and bubble column reactors. Chemical Engineering Science 47, 3297–3304.

Tchen, C.M., 1947. Mean value and correlation problems connected with the motion of small particles suspended in a turbulent fluid. D.Sc. Thesis, TU, Delft, The Netherlands.

Torvik, R., Svendsen, H.F., 1990. Modeling of slurry reactors: a fundamental approach. Chemical Engineering Science 45, 2325.

Tsuchiya, K., Furumoto, A., Fang, L.S., Zhang, J., 1997. Suspension viscosity and bubble rise velocity in liquid-solid fluidized beds. Chemical Engineering Science 52, 3053–3066.

van Baten, J.M., Krishna, R., 2001. Eulerian simulations for determination of the axial dispersion of liquid and gas phases in bubble columns operating in the churn-turbulent regime. Chemical Engineering Science 56, 503–512.

Wilkinson, P.M., 1991. Physical aspects and scale-up of high pressure bubble columns. D.Sc. Thesis, University of Groningen, The Netherlands.

Yang, Y.B., Devanathan, N., Dudukovic, M.P., 1992a. Liquid backmixing in bubble columns. Chemical Engineering Science 47, 2859–2864.

Yang, Y.B., Devanathan, N., Dudukovic, M.P., 1992b. Liquid backmixing in bubble columns. Chemical Engineering Science 47, 2859–2864.

Zhang, D.Z., Prosperetti, A., 1997. Momentum and energy equations for disperse two-phase flows and their closure for dilute suspensions. International Journal of Multiphase Flow 23, 425–453.